Bioorganic & Medicinal Chemistry 16 (2008) 8922–8931

Contents lists available at ScienceDirect

Bioorganic & Medicinal Chemistry

journal homepage: www.elsevier.com/locate/bmc

Distinctive molecular inhibition mechanisms for selective inhibitors of human 11β-hydroxysteroid dehydrogenase type 1

Hua Tu [a], Jay P. Powers [b,*,†], Jinsong Liu [c,‡], Stefania Ursu [a], Athena Sudom [c], Xuelei Yan [b], Haoda Xu [c], David Meininger [c], Michael DeGraffenreid [b], Xiao He [b], Juan C. Jaen [b,†], Daqing Sun [b], Marc Labelle [b,§], Hiroshi Yamamoto [d], Bei Shan [a], Nigel P. C. Walker [c], Zhulun Wang [c,*]

[a] Department of Metabolic Disorders, Amgen Inc., 1120 Veterans Boulevard, South San Francisco, CA 94080, USA
[b] Department of Medicinal Chemistry, Amgen Inc., 1120 Veterans Boulevard, South San Francisco, CA 94080, USA
[c] Department of Molecular Structure, Amgen Inc., 1120 Veterans Boulevard, South San Francisco, CA 94080, USA
[d] Chemical Research Laboratories, Central Pharmaceutical Research Institute, Japan Tobacco Inc., 1-1 Murasaki-cho, Takatsuki, Osaka 569-1125, Japan

ARTICLE INFO

Article history:
Received 8 April 2008
Revised 20 August 2008
Accepted 26 August 2008
Available online 29 August 2008

Keywords:
11β-Hydroxysteroid dehydrogenase (11β-HSD1)
Small molecule inhibitor
Inhibition mechanism
Enzyme kinetics
Crystal structure
X-ray crystallography

ABSTRACT

11β-hydroxysteroid dehydrogenase type 1 (11β-HSD1) catalyzes the NADPH dependent interconversion of inactive cortisone to active cortisol. Excess 11β-HSD1 or cortisol leads to insulin resistance and metabolic syndrome in animal models and in humans. Inhibiting 11β-HSD1 activity signifies a promising therapeutic strategy in the treatment of Type 2 diabetes and related diseases. Herein, we report two highly potent and selective small molecule inhibitors of human 11β-HSD1. While compound **1**, a sulfonamide, functions as a simple substrate competitive inhibitor, compound **2**, a triazole, shows the kinetic profile of a mixed inhibitor. Co-crystal structures reveal that both compounds occupy the 11β-HSD1 catalytic site, but present distinct molecular interactions with the protein. Strikingly, compound **2** interacts much closer to the cofactor $NADP^+$ and likely modifies its binding. Together, the structural and kinetic analyses demonstrate two distinctive molecular inhibition mechanisms, providing valuable information for future inhibitor design.

1. Introduction

Glucocorticoids are steroid hormones that are produced by the hypothalamus–pituitary–adrenal (HPA) axis as part of a normal stress response and have profound effects on blood glucose level and metabolism. Glucocorticoid excess in humans results in a variety of metabolic phenotypes, including glucose intolerance, central obesity, hypertension, dyslipidemia, and increased cardiovascular mortality, as seen in Cushing's Syndrome.[1] 11β-HSD1, widely expressed in tissues, is the principal enzyme that generates active glucocorticoids (cortisol) from inactive ones (cortisone) in a NADPH dependent manner, and has been proposed as an amplifier of glucocorticoid action.[2,3] Indeed, overexpression of 11β-HSD1 in the fat tissue of transgenic mice produced phenotypes similar to human metabolic syndrome, such as insulin-resistance, hyperlipidemia and hyperphagia.[4] The therapeutic benefit of inhibiting 11β-HSD1 activity has been demonstrated by treatment with the non-selective 11β-HSD inhibitor carbenoxolone in men with type 2 diabetes, in which carbenoxolone reduced the glucose production rate.[5] Furthermore, several selective small molecule 11β-HSD1 inhibitors have been recently shown to improve insulin sensitivity and metabolic syndrome in preclinical animal models.[6,7] Taken together, these results suggest that 11β-HSD1 is a promising pharmaceutical target for novel therapy in the clinical treatment of prevalent type 2 diabetes and other related metabolic disorders.[8–11]

The development of potent and selective small molecule inhibitors for 11β-HSD1 is currently being pursued vigorously by the pharmaceutical industry.[12–18] Overall, most compounds are active site inhibitors. However, their detailed kinetic and molecular mechanisms have not been reported to date. Here we present two novel and selective inhibitors of 11β-HSD1 as well as their kinetic and co-crystal structural analyses. The distinct molecular interactions and kinetic profiles of the different inhibitors revealed in this report provide the first detailed discussion, to our knowledge, of the molecular inhibition mechanism of 11β-HSD1 by small molecules.

* Corresponding authors. Tel.: +1 650 244 2446; fax: +1 650 837 9427 (Z.W.); tel.: +1 650 210 2949; fax: +1 650 625 8940 (J.P.P.).
E-mail addresses: jpowers@chemocentryx.com (J.P. Powers), zwang@amgen.com (Z. Wang).
† Present address: ChemoCentryx Inc., 850 Maude Avenue, Mountain View, CA 94043, USA.
‡ Present address: Guangzhou Institute of Biomedicine and Health, Guangzhou Science Park, 510663, China.
§ Present address: Lundbeck Research USA Inc., 215 College Road, Paramus, NJ 07652, USA.

0968-0896/$ - see front matter © 2008 Elsevier Ltd. All rights reserved.
doi:10.1016/j.bmc.2008.08.065

2. Results and discussion

2.1. Chemistry

In order to develop potent and selective small molecule inhibitors of human 11β-HSD1 enzyme activity, we performed high throughput screening of a small molecule compound library and optimized selected leads.[17–19] This effort resulted in two synthetic inhibitors, shown in Figure 1, which were derived from two distinct chemical series and were extensively characterized. Compound **1** is a representative of the sulfonamide series,[17] while compound **2** has the triazole moiety as its central chemical feature.[19] The synthesis of compound **1** (Scheme 1) began with reduction of the commercially available cyclopropyl ester **3** with sodium borohydride in a mixed (DME/MeOH) solvent system to give alcohol **4** in good yield. Alcohol **4** was then converted to its tosylate **5** by treatment with *p*-TsCl and triethylamine in dichloromethane. The crude tosylate **5** was directly converted to amine **6** by treatment with one equivalent of (*R*)-2-methylpiperazine in acetonitrile at 70 °C, and the resulting amine was then acylated with 4-acetylbenzenesulfonyl chloride to give *N*,*N*-disubstituted piperazine **7** in 36% overall yield from alcohol **4** (three steps). Ketone **7** was converted into a 1:1 diastereomeric mixture of trifluoromethylcarbinols **8** in excellent yield by treatment with $TMSCF_3$ and TBAF in THF. Resolution of the resulting diastereoisomers was accomplished by use of a carbamate chiral auxiliary. Formation of the mixed carbonate resulting from treatment of **8** with 4-nitrophenyl chloroformate and DMAP was followed by displacement of the nitrophenylphenol with commercially available (*S*)-(+)-2-amino-1-butanol in a single pot. The resulting mixture of diastereoisomers was separated via flash chromatography to give the pure desired diastereoisomer **9** in 35% yield from **8**. Treatment of **9** with KOH in *tert*-butanol at 90 °C gave compound **1** in good yield via hydrolysis of the nitrile to the primary amide with concomitant hydrolysis of the carbamate to the desired trifluoromethylcarbinol. Hydrolysis of the carbamate is believed to be facilitated by intramolecular cyclization of the auxiliary hydroxyl group to give the oxazolidinone, and is quite facile. We found that non-hydroxyl bearing amines used as the auxiliary carbamate may be hydrolyzed using the above method as well, albeit at a slower rate, presumably due to their inability to pass through the putative oxazolidinone.

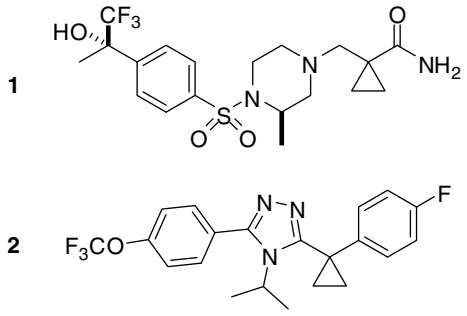

Figure 1. Chemical structures of compounds **1** and **2**.

The synthesis of compound **2** (Scheme 2) began with the cyclopropanation of commercially available benzonitrile **10** to give **11** in good yield. Amide formation via alkaline hydrolysis of the nitrile proceeded in excellent yield to give **12**, followed by acid hydrolysis to give acid **13**. Fischer esterification of the acid gave ester **14** in excellent overall yield. Treatment of ester **14** with hydrazine hydrate in refluxing ethanol afforded hydrazide **15**. Commercially available acid chloride **16** afforded benzamide **17** after treatment with 2-aminopropane in chloroform, and treatment of **17** with

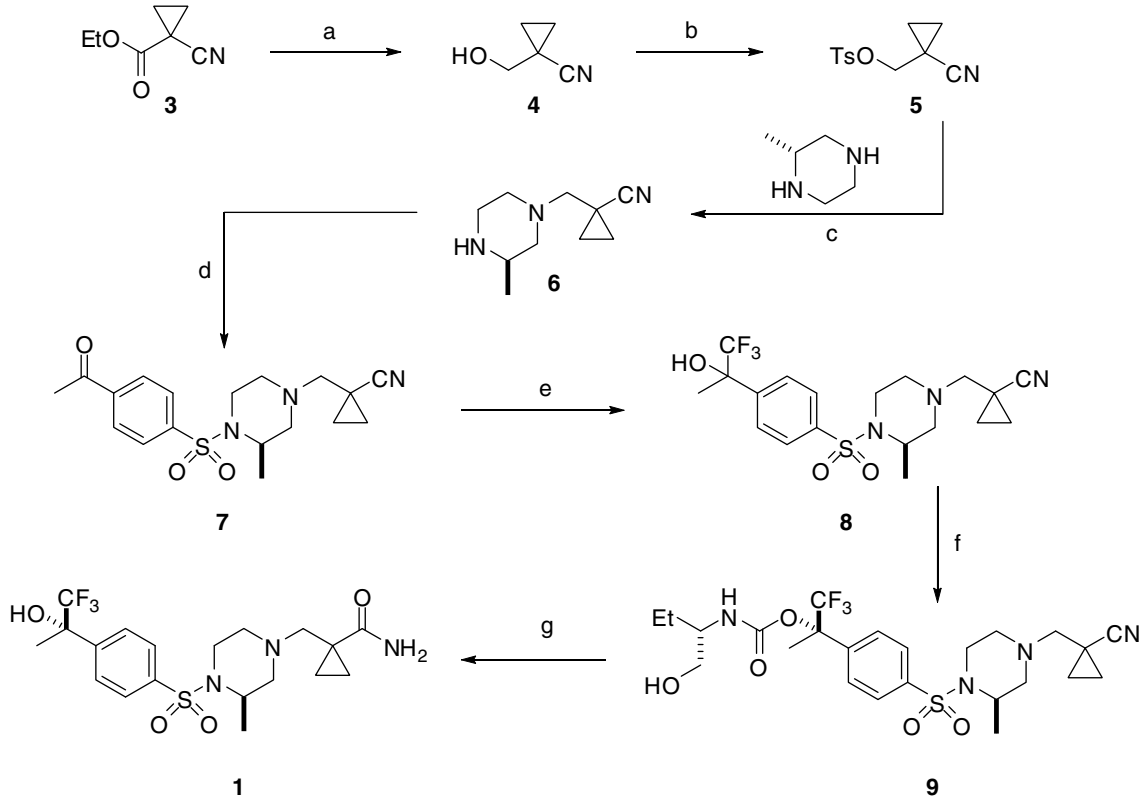

Scheme 1. Synthesis of compound **1**. Reagents: (a) $NaBH_4$, DME/MeOH, 74%. (b) *p*-TsCl, Et_3N, CH_2Cl_2. (c) (*R*)-(-)-2- Methylpiperazine, CH_3CN. (d) 4-Acetylbenzenesulfonyl chloride, Et_3N, CH_2Cl_2, yield 36% for steps b-d (**4** to **7**). (e) TMS-CF_3, TBAF, THF, yield 84%. (f) *i*. 4-Nitrophenyl chloroformate, DMAP, CH_3CN. *ii*. (*S*)-(+)-2-Amino-1-butanol. *iii*. Separation of the diastereoisomers via flash chromatography; yield of **9** from **8** 35%. (g) Potassium hydroxide, *tert*-butyl alcohol, 79%.

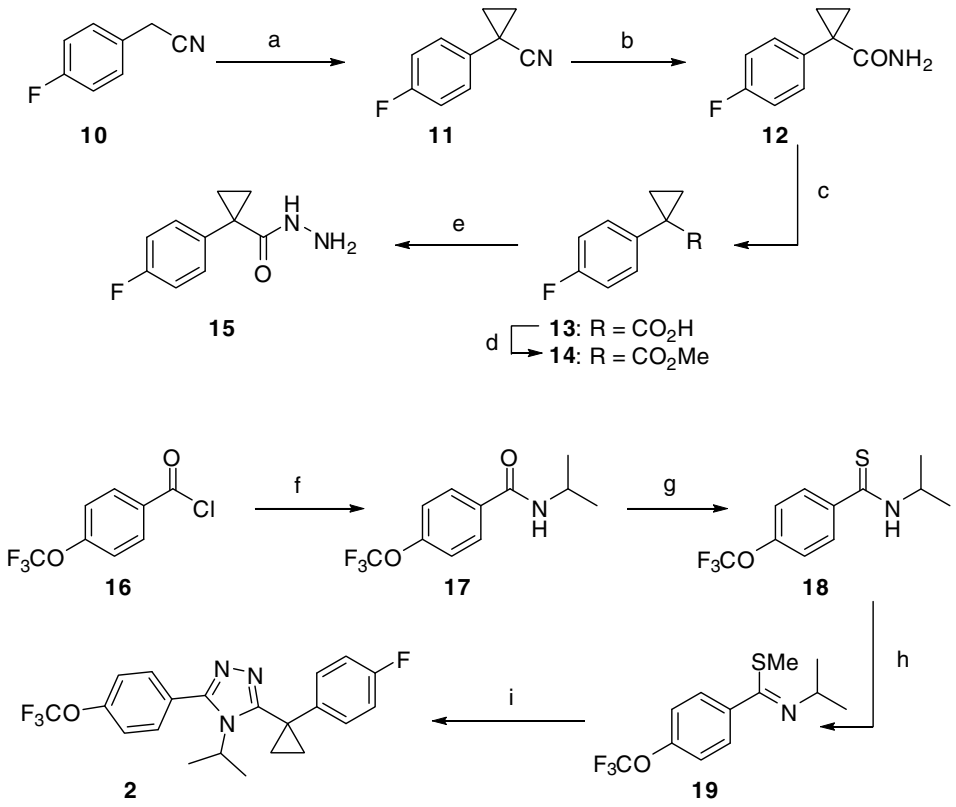

Scheme 2. Synthesis of compound **2**. Reagents and conditions: (a) 1-Bromo-2-chloroethane, benzyltriethylammonium chloride, NaOH, H_2O, 50 °C, 68%. (b) H_2O_2, NaOH, acetone/H_2O, 93%. (c) 6 N HCl, 1,4-dioxane, reflux, 98%. (d) Concentrated H_2SO_4, MeOH, reflux 8 h, quantitative. (e) Hydrazine hydrate, refluxing EtOH, 76%. (f) *Iso*-propylamine, $CHCl_3$, 0 °C, 93%. (g) Lawesson's reagent, THF, reflux, quantitative. (h) Methyl iodide, THF, 75%. (i) Compound 15, pyridine, reflux, 5 h, 35%.

Lawesson's reagent gave thioamide **18**, which was readily converted to thioimidate **19** in good yield. Combining thioimidate **19** in refluxing pyridine with hydrazide **15** afforded triazole inhibitor **2** in fair yield.

2.2. Inhibition of 11β-HSD1

Physiologically, 11β-HSD1 functions as a reductase enzyme (Figure 2A). We reconstituted an in vitro reductase assay with

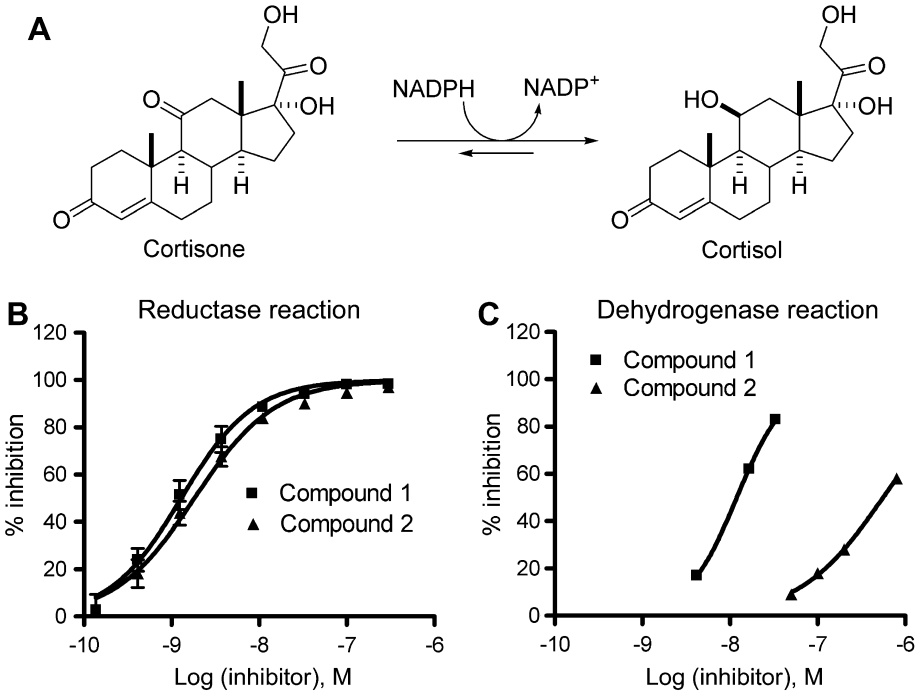

Figure 2. (A) Reaction scheme catalyzed by 11β-HSD1 reductase activity in vivo. Concentration–response curves for compounds **1** and **2** as inhibitors of 11β-HSD1 reductase (B) and dehydrogenase (C) activity. The reductase reaction was constituted with cortisone and cofactor NADPH, while the dehydrogenase reaction was made with cortisol and cofactor $NADP^+$.

recombinant full-length human 11β-HSD1 purified from a baculovirus expression system (Invitrogen) to measure the inhibitory potency of compounds **1** and **2**. Various concentrations of compound **1** and **2** were incubated with 11β-HSD1, [^{3}H]-cortisone and cofactor NADPH at 37 °C for 90 min in 96-well plate format. At the end of the incubation period, the reaction was stopped with the non-specific 11β-HSD1 inhibitor carbenoxolone, and the reaction product [^{3}H]-cortisol was captured and quantified by anti-cortisol monoclonal antibody in a scintillation proximity assay (SPA). Percent inhibition was calculated based on reference controls, and IC_{50} values were determined using a curve fitting algorithm based on percent inhibition and the corresponding compound concentrations. As shown in Figure 2B, both compound **1** and **2** could potently and completely inhibit the reductase reaction of 11β-HSD1. The biochemical IC_{50} is 1.2 ± 0.7 nM for compound **1**, and 1.6 ± 0.5 nM for compound **2**. Under similar assay conditions, neither compound **1** nor **2** significantly inhibited several related steroid enzymes, including human 11β-HSD2 and 17β-HSD1 at 10 μM, suggesting that both compounds are specific for 11β-HSD1.

Since 11β-HSD1 also has dehydrogenase activity in vitro, we measured the inhibitory activity of compounds **1** and **2** in the dehydrogenase assay as well. Reaction mixtures containing 11β-HSD1, [^{14}C]-cortisol, cofactor NADP and a range of compound concentrations were incubated at 37 °C for 1 h before being extracted with ethyl acetate. [^{14}C]-Cortisol and reaction product [^{14}C]-cortisone in the organic extract were then separated by thin layer chromatography (TLC), and were quantified with a phosphor-imager system. Percent inhibition was calculated based on references, and plotted against compound concentrations. As shown in Figure 2C, although compound **1** and **2** could both inhibit the dehydrogenase reaction of 11β-HSD1, the two compounds displayed very different inhibitory potency. Compound **2** appeared to be about 50-fold less potent than compound **1** in inhibiting the dehydrogenase reaction, while, as shown before, the two compounds had comparable potency in inhibiting the reductase reaction of the same enzyme. This set of data suggests that the two compounds have very different inhibition characteristics.

2.3. Kinetic analysis of inhibitors

Kinetic analysis was performed on the two compounds in vitro to understand their respective mechanisms of inhibition of 11β-HSD1. We used the same conditions as the aforementioned biochemical assays, but with either the cofactor NADPH or the substrate cortisol as a variable. Figure 3A shows the Lineweaver–Burk plot of compound **1** using NADPH as a variable, in which compound **1** decreased the apparent V_{max} of NADPH without affecting the K_m, indicating the inhibitor is non-competitive with respect to NADPH. As shown in Figure 3B, the secondary plot for reciprocal V_{max} as a function of compound **1** concentration yielded a K_i of 1.1 nM, similar to the IC_{50} value determined above. Figure 3C shows the Lineweaver–Burk plot of compound **1** in the presence of various concentrations of cortisol. Reciprocally, compound **1** increased the K_m for cortisol while leaving the V_{max} unchanged, demonstrating that enzyme inhibition by compound **1** is substrate-competitive and reversible. The secondary plot (Figure 3D) of apparent K_m as a function of compound **1** concentration yielded a K_i of 2.7 nM. These two sets of kinetic data complement each other and clearly suggest that compound **1** inhibits 11β-HSD1 by occupying its substrate binding site without affecting the cofactor NADPH binding.

A similar set of kinetic characterizations with compound **2**, however, showed considerably different profiles. As shown in Figure 3E of the Lineweaver–Burk plot of compound **2** with NADPH as a variable, compound **2** displayed a mixed inhibition profile with respect to NADPH with the value of alpha <1 (lines intersecting at a value of 1/V less than zero), indicating compound **2** decreased both the V_{max} and K_m of NADPH. Interestingly, in a substrate competition experiment (Figure 3F), compound **2** also showed a mixed inhibition profile with the value of alpha >1 (lines intersecting at a value of 1/V greater than zero), indicating compound **2** decreased V_{max} but increased K_m of substrate. These two complementary sets of kinetic data suggest that inhibition of 11β-HSD1 by compound **2** is much more complex than that of compound **1**, and cannot be completely overcome by an excess of either cofactor or substrate.

2.4. Co-crystal structures of 11β-HSD1 with inhibitors

To further elucidate the molecular mechanism of inhibition, we carried out structural analysis of 11β-HSD1 co-crystallized with inhibitors using X-ray crystallography. A truncated version of recombinant human 11β-HSD1 (residues 24–292 with a single mutation of C272S) was produced from *E. coli*. This 11β-HSD1 was purified in the presence of the steroidal detergent CHAPS (3-[(3-cholamidopropyl)dimethylammonio]-1-propanesulfonate). Crystals produced from this protein contained cofactor $NADP^+$ and CHAPS bound to the enzyme, although neither $NADP^+$ nor NADPH was supplemented during the purification and crystallization steps. Co-crystals of 11β-HSD1 with each inhibitor were then generated by soaking the 11β-HSD1 crystal with the inhibitors individually. The crystals belong to space group $P2_1$ with four protein molecules in the asymmetric unit which correspond to two dimers. The co-crystal structures of 11β-HSD1 in complex with compound **1** or compound **2** were determined by molecular replacement to 2.5 and 2.55 Å, respectively, using the previously reported 11β-HSD1 structure as a search model (PDB code: 1XU9).[20] The final electron density maps of 11β-HSD1 are clear, except for some disordered regions including the loop of residues 228 to 233 and the C-terminal loop of residues 281 to 292. The X-ray data statistics are shown in Table 1.

The overall structure of the 11β-HSD1 protein is similar to the one reported previously by Hosfield et al.[20] Resembling other short chain dehydrogenase/reductase (SDR) enzymes, the core structure of 11β-HSD1 (Figure 4) adopts a Rossmann fold with a central parallel 6-stranded β-sheet having 3 α-helices at each side.[21–23] In addition, 11β-HSD1 has an insertion of β6-α6 in an α-helix and extended-strand conformation, an extra β-strand (β7) packed in parallel with the β6 strand, and two C-terminal α-helices appended to the core structure. The cofactor $NADP^+$ shows well-defined electron density in the structure. The binding of $NADP^+$ is similar to that of other SDR enzymes, with the molecule in the same extended conformation as previously described, forming both extensive hydrophilic and hydrophobic interactions with the protein.[20,24,25]

The co-crystal structure of the 11β-HSD1 with inhibitor compound **1** showed well resolved electron density for compound **1** in all four protein molecules (Figure 5A). Compound **1** binds in a V-shaped conformation, snugly in the narrow steroid binding channel walled by the β6–α6 insertion at one side and the loop β5–α5 on the other side, with the trifluoromethyl hydroxyl phenyl moiety approaching the catalytic end of the substrate binding pocket and the cyclopropane carboxamide towards the solvent area where the C-terminal of an adjacent molecule in the crystal lattice packs. The inhibitor binding is almost identical in all four protein molecules. Compound **1** makes one direct hydrogen bond with 11β-HSD1 with one oxygen atom of the sulfonamide moiety accepting a proton from the backbone amide of Ala172 in loop β5–α5 (Figure 5B). The rest of the compound makes numerous van der Waals contacts with the protein, including residue Tyr183 from the catalytic Tyr-X-X-X-Lys motif. At the substrate recognition end, compound **1** also interacts with $NADP^+$, where the phenyl ring makes a van der Waals contact with the nicotinamide ring. In addition, the hydroxyl moiety forms a

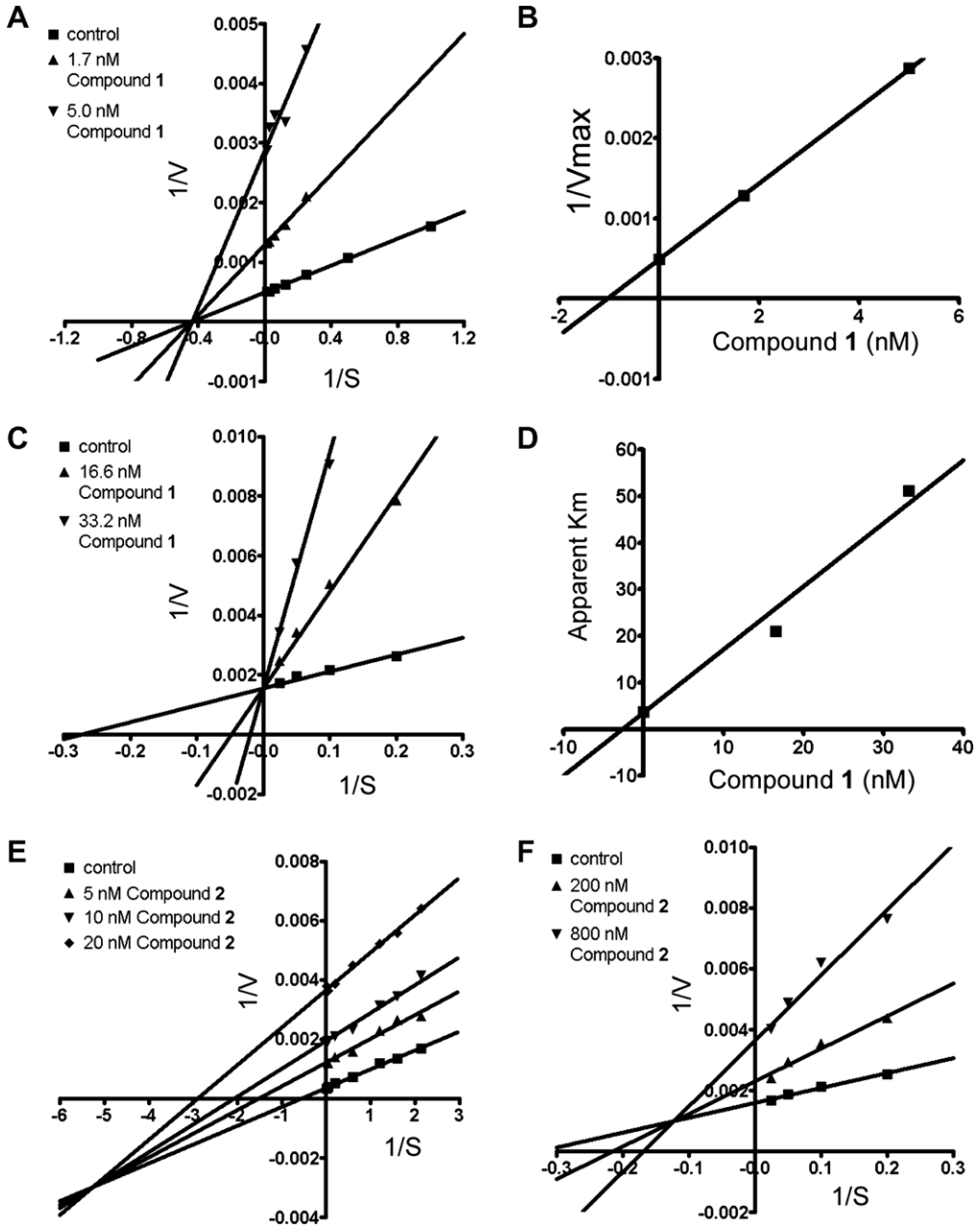

Figure 3. The primary (Lineweaver–Burk) and secondary plots of the kinetic assays. (A) Lineweaver–Burk plot of compound **1** with cofactor NADPH. (B) Secondary plot of K_i determination for compound **1** with NADPH. (C) Lineweaver–Burk plot of compound **1** with substrate cortisol. (D) Secondary plots of K_i determination for compound **1** with substrate cortisol. (E) Lineweaver–Burk plot of compound **2** with NADPH and (F) with substrate cortisol.

water-mediated hydrogen bond with one pyrophosphate oxygen of $NADP^+$. However, compound **1** does not change the binding state of $NADP^+$ to 11β-HSD1, which is consistent with our kinetic findings that compound **1** is non-competitive with NADPH.

In the co-crystal structure of 11β-HSD1 with compound **2**, the inhibitor also showed well-defined electron density in all four protein molecules (Figure 5C). Compound **2** is positioned in the steroid substrate binding site in an L-shaped conformation with the fluoro-phenyl group as the short arm, the cyclopropane moiety being the turning point, with triazole and trifluoromethoxy phenyl being on the long line (Figure 5D). Interestingly, the triazole moiety is situated right at the catalytic center, and makes two direct hydrogen bonds with residues Tyr183 and Ser170 of the catalytic triad (Ser170, Tyr183, and Lys187) responsible for substrate reduction. Each of the two unsubstituted nitrogen atoms of the triazole accepts a hydrogen bond from the hydroxyl moieties of Tyr183 and Ser170, respectively. In the parental crystal structure without inhibitor, where the steroid detergent molecule CHAPS occupies the substrate-binding site, the side chain of Ser170 points to Tyr183 as we previously observed in the compound **1** co-crystal structure (Figure 5B), with the hydroxyl moiety forming a hydrogen bond with Tyr183. The side chain of Tyr183 points to the cofactor $NADP^+$ and makes a hydrogen bond with one hydroxyl of the ribose. Here, the binding of compound **2** results in the Ser170 side chain rotating 180° and pointing away from Tyr183. The rest of the ligand–protein interactions are mainly hydrophobic in nature. The fluoro-phenyl moiety points towards the β4–α4 loop that passes on the top of the substrate-binding cleft. The phenyl ring makes van der Waals contacts with the side chains of Thr124 and Leu126, and the fluorine atom is in van der Waals contact with

Table 1
Data and refinement statistics[a]

Complex	11β-HSD1 + compound **1**	11β-HSD1 + compound **2**
Crystal wavelength (Å)	1.54	1.0
Space group	$P2_1$	$P2_1$
Cell constants	a = 56.6 Å, b = 153.8 Å, c = 73.9 Å, β = 93.1	a = 56.7 Å, b = 153.3 Å, c = 73.6 Å, β = 92.2
Resolution (Å)	2.5	2.55
Total reflections	100,110	147,508
No. of unique reflections	40,775	40,780
Completeness (%) (outer shell)	93.7 (89.7)	99.8 (100.0)
R_{sym} (%) (outer shell)	12.3 (16.4)	4.3 (44.2)
I/σ (outer shell)	3.9 (3.8)	10.2 (1.6)
R_{cryst} (%)	21.0	21.8
R_{free} (%)	28.9	27.8
RMS deviations: Bonds (Å)	0.014	0.020
RMS deviations: Angles (deg)	1.65	2.10
Total non-H atoms	8758	8447

$R_{sym} = \sum|I_{avg} - I_j|/\sum I_j$.
$R = \sum|F_o - F_c|/\sum F_o$, where F_o and F_c are observed and calculated structure factors, respectively, R_{free} was calculated from a randomly chosen 5% of reflections excluded from the refinement, and R_{cryst} was calculated from the remaining 95% of reflections.

[a] RMS deviation is the root-mean-square deviation from ideal geometry. Numbers in parentheses are for the highest resolution shell.

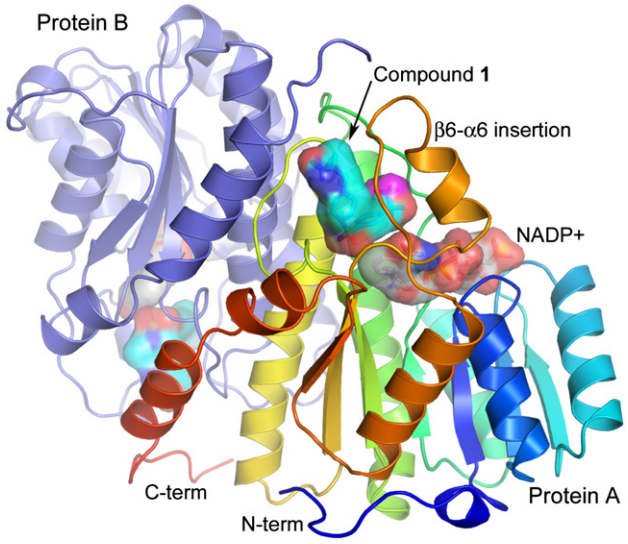

Figure 4. Overall co-crystal structure of 11β-HSD1 with compound **1**. The protein is shown as a ribbon diagram, spectrum color coded with N-terminal colored in blue to C-terminal in red. The cofactor NADP$^+$ and compound **1** are shown in a molecular surface representation which is color coded red for oxygen, blue for nitrogen, orange for phosphorus, magenta for fluorine and cyan for carbon in compound **1** and grey for carbon in NADP$^+$. The dimer partner is shown with a purple ribbon.

the backbones of Ser125 and Leu126. The trifluoromethoxy phenyl is oriented towards the solvent area with the trifluoromethoxy group occupying the space normally occupied by the side chain of Tyr177. As a result, Tyr177 swings up and adopts a different side chain conformation as compared with the parental structure and the compound **1** co-crystal structure.

In addition to the above ligand–protein interactions, we observed that the electron density of compound **2** connects to the density of NADP$^+$ with the triazole edge stacking on the nicotinamide ring (Figure 6). The distances between the two unsubstituted nitrogen atoms of the triazole to the C4 and C5 atoms of the nicotinamide ring are merely 3.0 Å, respectively, which are less than the conventional van der Waals distance between C and N atoms. While compound **1** occupies only the substrate site and is in van der Waals contact with NADP$^+$, compound **2** not only resides in the substrate site and engages in interactions with two residues of the catalytic triad, but also impinges partially on the cofactor site. Interactions of the triazole ring of compound **2** with the two catalytic residues evidently lessen the interactions of these residues with NADP$^+$. However, this is most likely compensated for by the interactions between NADP$^+$ and the anchored compound **2**. Together, this set of interactions likely increased the affinity of NADP(H) to 11β-HSD1, a conclusion which is supported by the kinetic analysis.

3. Conclusion

In summary, we have reported two novel 11β-HSD1 inhibitors and their molecular interactions with 11β-HSD1 by kinetic analysis and X-ray crystallography. The structures revealed that a set of amino acid residues in the active site, including Ala172 and the catalytic triad Ser170, Tyr183, and Lys187, makes important interactions with inhibitors and is therefore the key determinant of binding affinity for these small molecule inhibitors. The two compounds presented here are of different inhibitor classes, as shown by their chemical structures and kinetic profiles, as well as two different binding modes, even though they both occupy the steroid substrate binding site. Compound **1** behaves as a simple substrate competitive inhibitor. Structurally, it occupies the substrate-binding site and neither perturbs the catalytic site nor affects the NADP(H) binding. In contrast, compound **2** inhibits 11β-HSD1 in a mixed inhibitor mode. Structurally, it not only occupies the substrate binding site but also alters the catalytic site residues and NADP(H) binding. Furthermore, compound **2** imposes tight interactions with NADP$^+$, enlightening the observed kinetic profile of a mixed inhibitor.

NADPH is an essential cofactor for the 11β-HSD1 reduction reaction. Recent literature has shown that local NADPH concentration generated by hexose-6-phosphate dehydrogenase (H6PD) might be critical for the reductase activity of 11β-HSD1, which is confined to the ER lumen.[26] In fact, H6PD deficiency results in a marked reduction of 11β-HSD1 activity.[26] Thus, the coupled modulation of compound **2** on both substrate and NADP(H) binding is noteworthy for further investigation. Conceivably, the two inhibition mechanisms might yield distinct in vivo efficacy profiles, which might be an interesting subject for future studies. Our results provide important insight into both the inhibition mechanism of 11β-HSD1 and future inhibitor design.

4. Experimental

Reagents and solvents used below were obtained from commercial sources and when required were purified in the accepted fashion. ^{1}H NMR spectra were obtained on a Varian Gemini 400 MHz NMR spectrometer. Electrospray ionization (ESI) mass spectrometry analysis was performed using a Hewlett-Packard 1100 MSD electrospray mass spectrometer using the HP1100 HPLC for sample delivery. Combustion analyses were performed by Atlantic Microlab Inc. (Norcross, GA). Air and/or moisture sensitive reactions were carried out under N_2 using flame dried glassware and standard syringe/septa techniques.

4.1. Synthesis of (1-(((*R*)-3-methyl-4-(4-((*S*)-1,1,1-trifluoro-2-hydroxypropan-2-yl)phenylsulfonyl)-piperazin-1-yl)methyl)-cyclopropanecarboxamide) (1)

1-(Hydroxymethyl)cyclopropanecarbonitrile (**4**): To a solution of 48.19 g 1-cyanocyclopropanecarboxylic acid ethyl ester

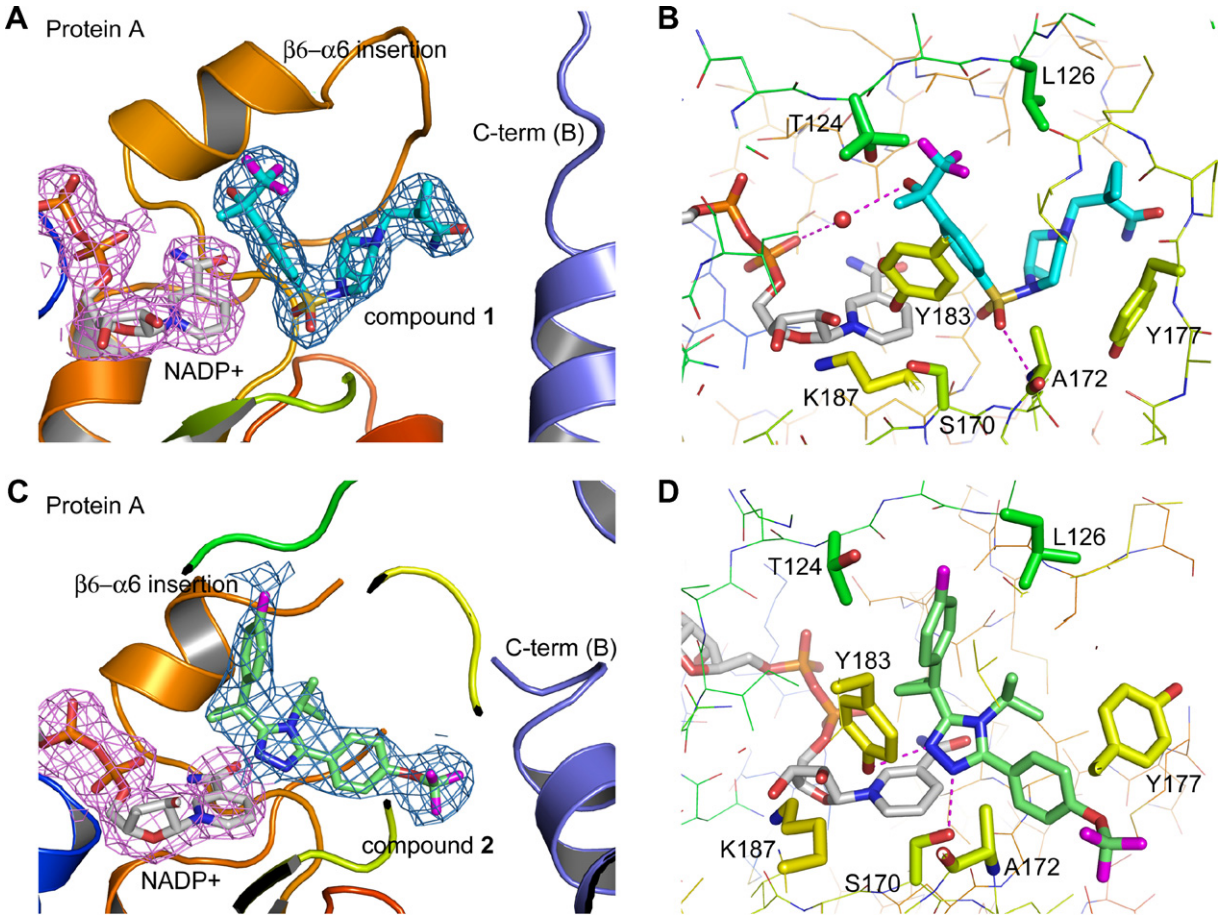

Figure 5. The inhibitor binding mode of 11β-HSD1. (A) Compound **1**, shown in stick representation, in the active site. Electron density maps, shown in blue and magenta for compound **1** and NADP$^+$, respectively, are contoured at a level of 1σ from a $2F_o-F_c$ map. (B) Protein–ligand interactions for compound **1**. (C) Compound **2,** shown in stick representation with carbon atoms in light green, in the active site. Electron density maps, shown in blue and magenta for compound **2** and NADP$^+$, respectively, are contoured at a level of 1σ from a $2F_o-F_c$ map. (D) Protein–ligand interactions for compound **2**. The hydrogen bonds are shown in magenta dotted lines. Coloring is as in Figure 4.

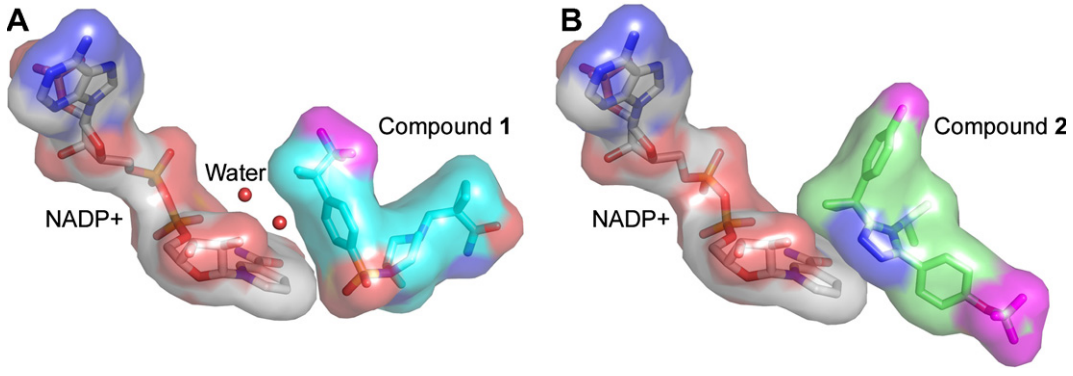

Figure 6. The interactions between inhibitor and cofactor NADP$^+$, shown in molecular surface representation. (A) Compound **1** and (B) compound **2**. Coloring is as in Figure 5.

(0.35 mol, 1.0 equiv) in 200 mL ethylene glycol dimethyl ether and 20 mL MeOH was added 26.2 g $NaBH_4$ (0.69 mol, 2.0 equiv) in portions at 0 °C. The reaction mixture was stirred at room temperature for 24 h, followed by the dropwise addition of 50 ml sat. NH_4Cl to the reaction mixture at 0 °C. The resulting suspension was stirred at room temperature for 24 h, filtered, and the solid was washed with 10% MeOH/DME. The solid was then acidified with 2 N HCl at 0 °C to pH 6–7 and further extracted with 10% MeOH/CH_2Cl_2. The organic layers were then combined, dried ($MgSO_4$), and concentrated under reduced pressure. Purification by distillation (bp 85–87 °C @ 5–10 mm Hg) gave 25.0 g of the product as a colorless oil (0.26 mol, 74%): ^{1}H NMR (DMSO-d_6, 400 MHz) δ 3.39 (d, J = 6.0 Hz, 2 H), 1.14 (m, 2H), 0.92 (m, 2H).

(1-Cyanocyclopropyl)methyl-4-methylbenzenesulfonate (**5**): To 150 g of the 1-(hydroxymethyl)-cyclopropanecarbonitrile **4** (prepared above, 154 mmol, 1.0 equiv) in 3.0 L CH_2Cl_2 was added 311.7 g triethylamine (3.08 mol, 2.0 equiv) and 324.7 g *p*-toluenesulfonyl chloride (1.7 mol, 1.1 equiv) at 0 °C. The solution was allowed to stir at 0 °C for 15 min, and then at room temperature for an additional 18 h. The solution was then re-cooled and 20 ml

2-(dimethylamino)ethanol was added to the reaction mixture at 0 °C, which was then allowed to stir for an additional 2 h. 1.5 L 1 N HCl was added and the resulting solution was stirred for an additional 30 min. The organic phase was separated, washed (1× 1 N HCl, 1× H_2O, 1× sat. $NaHCO_3$), dried (Na_2SO_4), and concentrated under reduced pressure to give 254 g of the crude product tosylate **5** as light brown solid.

(*R*)-1-((3-Methylpiperazin-1-yl)methyl)cyclopropanecarbonitrile (**6**): The crude tosylate **5** obtained above (252 g, 1.0 mol, 1.0 equiv) in 1.2 L CH_3CN was combined in a 3 L flask with 200 g (*R*)-(−)-2-methylpiperazine (2.0 mol, 2.0 equiv). The resulting mixture was then placed into a preheated 70 °C bath. After stirring for 12 h, the mixture was cooled to room temperature and concentrated under reduced pressure. The resulting residue was diluted with sat. $NaHCO_3$, extracted (3× 10% MeOH/CH_2Cl_2), dried ($MgSO_4$), and concentrated under reduced pressure. The resulting amine (**6**) was taken directly to the next step without any additional purification.

(*R*)-1-((4-(4-Acetylphenylsulfonyl)-3-methylpiperazin-1-yl)-methyl)cyclopropanecarbonitrile (**7**): The crude amine **6** obtained above was dissolved in 1.5 L CH_2Cl_2 followed by the addition of 202 g triethylamine (2.0 mol) at 0 °C. Two hundred grams of 4-acetylbenzenesulfonyl chloride was then added to the reaction mixture in portions. After the reaction appeared complete as monitored via TLC, the resulting mixture was diluted with sat. $NaHCO_3$ and stirred for an additional 2 h. The organic phase was separated, and the aqueous solution was extracted (4× 10% MeOH/CH_2Cl_2). The organics were then combined, dried ($MgSO_4$), and concentrated under reduced pressure. The crude product was passed through a plug of SiO_2 (50% EA/hexanes), followed by purification of the resulting white solid by crystallization (1.2 L 50% EtOAc/hexanes) to give 200 g of the product **7** as a white solid (55.3 mol, 36% for three steps): ^{1}H NMR (DMSO-d_6, 500 MHz) δ 8.14 (d, J = 8.0 Hz, 2H), 7.95 (d, J = 8.5 Hz, 2H), 4.05 (m, 1H), 3.63 (m, 1H), 3.18 (ddd, J = 12.5, 6.0, 3.0 Hz, 1H), 2.85 (d, J = 11.5 Hz, 1H), 2.74 (d, J = 11.5 Hz, 1H), 2.65 (s, 3H), 2.46 (d, J = 13.0 Hz, 1H), 2.21 (d, J = 13.0 Hz, 1H), 2.04 (dd, J = 11.0, 3.5 Hz, 1H), 1.94 (ddd, J = 11.5, 5.8, 3.5 Hz, 1H), 1.20 (m, 2H). 1.10 (dd, J = 15.0, 7.5 Hz, 3H), 0.85 (m, 2H); MS (ESI): m/z = 362.2 $[M+H]^+$.

1-(((*R*)-3-Methyl-4-(4-(1,1,1-trifluoro-2-hydroxypropan-2-yl)-phenylsulfonyl)piperazin-1-yl)methyl)cyclopropanecarbonitrile (**8**): To a 2 L flask containing a portion of ketone **7** obtained above (165 g, 45.6 mmol, 1.0 equiv) in 900 mL THF was added 97.2 g TMS-CF_3 (68.4 mmol, 1.5 equiv) at 0 °C. The solution was allowed to stir for 30 min. Tetrabutylammonium fluoride (684 mL, 1.0 M in THF, 68.4 mmol, 1.5 equiv) was added dropwise via addition funnel over a period of 3 h. After the addition was complete, the solution was allowed to stir for an additional 30 min and warm to room temperature, followed by the addition of sat. $NaHCO_3$, and the resulting mixture was allowed to stir overnight. The organic phase was separated and the aqueous solution was extracted (4× 10% MeOH/CH_2Cl_2). The organics were combined, dried ($MgSO_4$), and concentrated under reduced pressure. Purification by flash chromatography (SiO_2, 50% EtOAc/hexanes) gave 165 g of the product **8** as white solid (38.2 mol, 84%): ^{1}H NMR (DMSO-d_6, 500 MHz) δ 7.84 (m, 4 H), 6.86 (s, 1H), 4.01 (m, 1H), 3.58 (m, 1H), 3.16 (ddd, J = 13.0, 6.5, 3.0 Hz, 1H), 2.85 (d, J = 11.0 Hz, 1H), 2.73 (d, J = 11.0 Hz, 1H), 2.45 (d, J = 13.0 Hz, 1H), 2.21 (d, J = 13.0 Hz, 1H), 2.05 (dd, J = 11.5, 3.5 Hz, 1H), 1.95 (ddd, J = 11.5, 5.8, 3.5 Hz, 1H), 1.73 (s, 3H), 1.20 (m, 2H). 1.09 (d, J = 7.0 Hz, 3H), 0.86 (m, 2H); MS (ESI): m/z = 432.1 $[M+H]^+$.

(*S*)-2-(4-((*R*)-4-((1-Cyanocyclopropyl)methyl)-2-methylpiperazin-1-ylsulfonyl)phenyl)-1,1,1-trifluoropropan-2-yl (*S*)-1-hydroxybutan-2-ylcarbamate (**9**): To a 2 L flask containing product **8** obtained above (160 g, 37.1 mmol, 1.0 equiv) in 465 mL CH_3CN was added 67.9 g DMAP (55.6 mol, 1.5 equiv) at 0 °C, followed by the addition of 4-nitrophenyl chloroformate (89.7 g, 44.5 mol, 1.2 equiv) in portions. The resulting mixture was allowed to stir for 15 min at 0 °C followed by 5.5 h at room temperature. 56.2 g (*S*)-(+)-2-amino-1-butanol (63.1 mmol, 1.7 equiv) was added dropwise via addition funnel. After the addition was complete, the solution was allowed to stir for an additional 12 h. Most of the CH_3CN was removed under reduced pressure and the residue was diluted with EtOAc. The solid was filtrated off and washed with EtOAc. The combined liquids were then washed with sat. NH_4Cl, dried ($MgSO_4$), and concentrated under reduced pressure. The two diastereomers obtained were purified and separated by flash chromatography (SiO_2, 50% EtOAc /hexanes). The first portion of the two close spots was collected and concentrated under reduced pressure to give 70 g of the desired pure diastereomer **9** as colorless oil (12.8 mmol, 34.5%).

1-(((*R*)-3-Methyl-4-(4-((*S*)-1,1,1-trifluoro-2-hydroxypropan-2-yl)phenylsulfonyl)piperazin-1-yl)methyl)cyclopropanecarboxamide (**1**): A 500 mL flask containing product **9** obtained above (70.0 g, 12.8 mmol) was charged with 300 mL *t*-BuOH and 50.0 g KOH. The resulting mixture was then placed into a preheated 90 °C bath. After stirring for 12 h, the mixture was diluted with H_2O, and extracted (5× 10% MeOH/CH_2Cl_2). The organics were then dried ($MgSO_4$) and concentrated under reduced pressure. Purification by flash chromatography (SiO_2, 90% EtOAc /hexanes) gave 50.0 g of the product as white solid (11.1 mmol, 87%, 88% ee). The white solid was then dissolved in 800 mL boiling CH_3CN and the resulting solution was allowed to cool overnight in an open flask. The crystals which formed overnight were filtered. The filtrate was then concentrated under reduced pressure to give 46.0 g of the final product as a white solid (10.2 mmol, 79% overall yield, 94% ee): mp 169–172 °C; ^{1}H NMR (DMSO-d_6, 400 MHz) δ 8.02 (s, 1H), 7.83 (m, 4H), 7.00 (s, 1H), 6.86 (s, 1H), 4.02 (m, 1H), 3.59 (m, 1H), 3.17 (t, J = 12.0 Hz, 1H), 2.90 (d, J = 11.0 Hz, 1H), 2.76 (d, J = 11.5 Hz, 1H), 2.42 (d, J = 13.0 Hz, 1H), 2.23 (d, J = 13.0 Hz, 1H), 1.93 (dd, J = 3.5, 11.5 Hz, 1H), 1.79 (m, 1H), 1.73 (s, 3H), 1.03 (d, J = 6.5 Hz, 3H), 0.96 (d, J = 3.0 Hz, 2H), 0.43 (d, J = 3.0 Hz, 2H); ^{13}C NMR (100 MHz, DMSO-d_6) δ 174.3, 144.4, 140.2, 127.6, 126.5, 73.4, 73.1, 61.5, 56.7, 51.7, 48.8, 22.6,19.7, 15.1, 13.4, 13.0; IR (neat, cm^{-1}) 3448, 3138, 1647, 1589, 1421, 1338, 1281, 1169, 1150, 1094, 981, 761, 713; MS (ESI): m/z = 450 $[M+H]^+$; Anal. calcd for $C_{19}H_{26}F_3N_3O_4S$: C, 50.77; H, 5.83; N, 9.35. Found: C, 50.52; H, 5.88; N, 9.14; $[\alpha]^{25}_D$-38° (c 0.50, CH_2Cl_2).

4.2. Synthesis of (3-(1-(4-fluorophenyl)cyclopropyl)-4-isopropyl-5-(4-(trifluoromethoxy)phenyl)-4H-1,2,4-triazole) (2)

To a mixture of 1-(4-fluorophenyl)acetonitrile 10 (20.3 g, 150 mmol), 1-bromo-2-chloroethane (25 mL, 300 mmol) and benzyltriethylammonium chloride (683 mg, 3.00 mmol) was added 50% aqueous NaOH (84 g, 1.05 mol), and the resulting mixture was heated at 50 °C overnight. After cooling, the mixture was poured into water and extracted with diisopropyl ether. The organic layer was washed sequentially with water, 1 N aqueous HCl, and brine, and dried over $MgSO_4$. Filtration, concentration in vacuo and purification by silica gel flash chromatography (*n*-hexane/EtOAc 6:1) gave 16.4 g (68%) of 11 as a yellow oil: ^{1}H NMR ($CDCl_3$, 400 MHz) δ *7.25–7.33* (m, 2H), 7.01–7.10 (m, 2H), 1.70–1.76 (m, 2H), 1.35–1.41 (m, 2H).

To a solution of **11** (16.4 g, 102 mmol) in acetone (140 mL) was added 4 N aqueous NaOH (100 mL) at room temperature. 30% H_2O_2 (150 mL) was added dropwise to the solution with cooling in an ice-water bath. The mixture was allowed to stand at room temperature and stirred for an additional 2 h. The reaction mixture was cooled in an ice-water bath, and aqueous Na_2SO_3 (10% in water, 159 mmol) was added to the mixture. The solvent was removed

by evaporation in vacuo, and the precipitated solid was collected by filtration and washed with water and *n*-hexane to give 17.0 g (93%) of 12 as a white solid.

A mixture of **12** (17.0 g, 94.8 mmol) in 6 N aqueous HCl (95 mL) and 1,4-dioxane (150 mL) was heated at reflux temperature overnight. The solvent was removed by evaporation in vacuo, and the residue extracted with EtOAc. The organic layer was washed with brine and dried over $MgSO_4$. Filtration and concentration in vacuo gave 16.8 g (98%) of the product **13** as a white solid: ^{1}H NMR (DMSO-d_6, 400 MHz) δ 12.3 (broad s, 1 H), 7.30–7.38 (m, 2H), 7.05–7.14 (m, 2H), 1.42–.47 (m, 2H), 1.10–1.15 (m, 2H); MS (ESI): m/z = 179.1 $[M-H]^-$.

A mixture of **13** (11.8 g, 65.5 mmol) and concentrated H_2SO_4 (1.5 mL) in MeOH (100 mL) was heated at reflux temperature for 8 h. The solvent was removed by evaporation in vacuo. The residue was diluted with water and extracted with EtOAc. The organics were washed sequentially with sat. aqueous $NaHCO_3$, water, and brine, and dried over $MgSO_4$. Filtration and concentration in vacuo gave 12.7 g (quantitative) of **14** as yellow oil.

A mixture of **14** (12.7 g, 65.5 mmol) and hydrazine hydrate (12.7 mL, 328 mmol) in EtOH (40 mL) was heated at reflux temperature overnight. The solvent was removed by evaporation in vacuo, and the residue was crystallized from water and collected by filtration to give 9.64 g (76%) of **15** as a pale yellow solid: ^{1}H NMR (DMSO-d_6, 300 MHz) δ 8.10 (s, 1H), 7.30–7.38 (m, 2H), 7.08–7.17 (m, 2H), 4.16 (s, 2H), 1.28–1.35 (m, 2H), 0.90–0.97 (m, 2H).

To a solution of isopropylamine (6.83 mL, 80.2 mmol) in chloroform (15 mL) was added 4-trifluoromethoxybenzoyl chloride **16** (3.60 g, 16.0 mmol) over 5 min with cooling in an ice-water bath. The reaction mixture was stirred for 30 min and concentrated in vacuo. The residue was washed in sat. aqueous $NaHCO_3$ and collected by filtration to give 3.69 g (93%) of **17** as a white solid.

A mixture of **17** (3.69 g, 14.9 mmol) and Lawesson's reagent (4.83 g, 11.9 mmol) in THF (40 mL) was heated at reflux temperature for 1 h. After cooling, the mixture was diluted with EtOAc and the insoluble material was removed by filtration. The filtrate was washed with sat. aqueous $NaHCO_3$ and brine, and dried over $MgSO_4$. Filtration, concentration in vacuo, and purification by silica gel chromatography (*n*-hexane/EtOAc 5:2) gave 4.00 g (quantitative yield) of 18 as a yellow solid.

To a solution of **18** (4.00 g, 15.2 mmol) in THF (40 mL) was added methyl iodide (3.78 mL, 60.7 mmol). The solution was stirred for 60 h at room temperature and concentrated in vacuo. The residue was triturated in EtOAc and collected by filtration to give 4.67 g (75%) of **19** as a solid.

A mixture of **15** (1.00 g, 5.15 mmol) and **19** (2.50 g, 6.17 mmol) in pyridine (10 mL) was heated at reflux temperature for 5 h. The solvent was removed by evaporation in vacuo, and the residue extracted with EtOAc. The organic layer was washed with sat. aqueous $NaHCO_3$ and brine, and dried over $MgSO_4$. Filtration, concentration in vacuo and purification by silica gel chromatography ($CHCl_3$/acetone 5/1:1/1) gave 745 mg (35%) of product **2** as a white solid: mp 144–146 °C;^{1}H NMR (DMSO-d_6, 400 MHz) δ 7.65 (m, 2H), 7.51 (d, J = 7.8 Hz, 2H), 7.22–7.12 (m, 4H), 4.52 (m, 1H), 1.57 (m, 2H), 1.46 (m, 2H), 0.97 (d, J = 6.6 Hz, 6H); ^{13}C NMR (100 MHz, DMSO-d_6) δ 161.9, 159.6, 156.2, 149.3, 137.6, 132.5, 129.1, 128.2, 128.1, 120.7, 115.5, 115.2, 47.8, 21.7, 20.2, 15.3; IR (neat, cm^{-1}) 3001, 2362, 2334, 1655, 1510, 1473, 1420, 1258, 1222, 1165, 830, 810; MS (ESI): m/z = 406 $[M+H]^+$; Anal. calcd for $C_{21}H_{19}F_4N_3O$: C, 62.22; H, 4.72; N, 10.37. Found: C, 62.19; H, 4.70; N, 10.42.

4.3. Biochemical assays

Full-length human 11β-HSD1 was cloned, tagged with a FLAG sequence at the C-terminus, and expressed in Hi5 cells via a baculovirus protein expression system. Cells infected with the 11β-HSD1-expressing baculovirus were extracted with lysis buffer (50 mM Tris, pH 7.5, 150 mM NaCl, 0.5% Triton). FLAG-tagged 11β-HSD1 was captured by anti-FLAG tagged beads (Sigma), eluted with a FLAG peptide (Sigma), and used as the enzyme source in the biochemical assays for potency determination and kinetic analysis.

To determine the inhibitory activity and IC_{50} values (the inhibitor concentrations giving 50% inhibition) in the reductase assay, inhibitors of various concentrations were incubated with 100 μl/well PBS buffer containing 10 ng of purified human 11β-HSD1, 0.1% BSA (Sigma), 16 nM [^{3}H]-cortisone (GE Healthcare, 1.8TBg/mol, 49 Ci/mmol) and 500 μM NADPH (Sigma) in 96-well plates at 37 °C for 90 min. At the end of reaction incubation, 40 μl PBS buffer containing 175 μM 11β-HSD1 inhibitor carbenoxolone (Sigma), 0.16 μg of anti-cortisol monoclonal antibody (East Coast Biologics) and 365 μg of SPA PVT anti-mouse antibody-binding beads (GE Healthcare) were added to each well to stop the enzyme reaction and capture [^{3}H]-cortisol to the SPA beads. The reaction product [^{3}H]-cortisol in each well was determined with a TopCount microscintillation plate reader (Packard Instrument). Percent inhibition was calculated based on references set with no compound as 0% inhibition and 100 μM carbenoxolone as 100%. IC_{50} values were determined using curve fitting algorithm Prism (GraphPad) based on percent inhibition and the corresponding inhibitor concentrations.

To determine the inhibitory activity in the dehydrogenase assay, a range of concentrations of each inhibitor were added to wells containing 100 μl of PBS buffer containing 10 ng human 11β-HSD1, 0.1% BSA and 100 μM NADP, 2.25 μM unlabeled cortisol (Sigma) and 0.25 μM [^{14}C]-cortisol (Perkin-Elmer Life Sciences, 1.67–2.22 GBg/mmol, 45–60 mCi/mmol). After a 1-h incubation at 37 °C, the reaction mix was extracted with ethyl acetate. [^{14}C]-Cortisone and [^{14}C]-cortisol in the organic phase were separated by thin layer chromatography, and were quantified with a phosphor-imager system (Fujifilm). Percent inhibition was calculated based on references set with no compound as 0% inhibition and 100 μM carbenoxolone as 100%.

4.4. Kinetic analysis of NADPH and substrate competition

To determine the mechanism of kinetic action using NADPH concentration as a variable, various concentrations of NADPH were incubated in each well of a 96-well plate with 100 μl of PBS buffer containing 10 ng human 11β-HSD1, 0.1% BSA, and 16 nM of [^{3}H]-cortisone with or without inhibitors in the aforementioned 96-well assay. After 90-min incubation at 37 °C, [^{3}H]-cortisol was captured by the anti-cortisol monoclonal antibody and quantified with the scintillation proximity assay. Lineweaver–Burk double-reciprocal plots were generated from the range of NADPH concentrations and the corresponding reaction velocity of cortisol formation to produce apparent K_m and V_{max}.

Kinetic studies examining the dehydrogenase activity of 11β-HSD1 were performed by incubating various concentrations of [^{14}C]-labeled cortisol with 10 ng human 11β-HSD1, 0.1% BSA and 100 μM NADP, with or without inhibitors in 100 μl/well of PBS buffer. After 1-h incubation at 37 °C, the reaction mix was extracted with ethyl acetate. [^{14}C]-Cortisone and [^{14}C]-cortisol in the organic phase were separated by thin layer chromatography, and were quantified with a phosphor-imager system (Fujifilm). Apparent K_m and V_{max} values were derived from Lineweaver–Burk double-reciprocal plot analysis.

4.5. Protein preparation and crystallization

The protein preparation was carried out according to a previously reported protocol.[20] In brief, the truncated form of human 11β-HSD1

(residue 24–292) with a single mutation C272S was cloned into a pBAD-ThioE vector (Invitrogen) by PCR. The recombinant protein with a N-terminal affinity tag of MKHQHQHQHQHQQPL was expressed in *E. coli* Rossetta1(DE3) cells (Novagen), grown in 2YT medium at 30 °C and induced by 0.2% arabinose and 0.25 mM corticosterone overnight at 20 °C before harvesting. The protein was purified by a Ni^{+}–NTA column (Qiagen), and eluted with 200 mM imidazole after a wash with 40 mM imidazole. The Ni+ eluant was then applied to a superdex 200 column (Pharmacia). The protein eluted as a dimer in a buffer of 250 mM NaCl, 25 mM Tris–HCl, pH 7.9, and 4 mM CHAPS and was then concentrated to 30 mg/mL for crystallization. The 11β-HSD1 crystals were grown at 16 °C in a sitting drop with 3 μl of the protein solution and 3 μl of the well solution containing 16-18% (w/v) PEG3350 and 0.1 M MES (pH 6.2–6.4). The inhibitors were introduced into the crystals by a soaking method. The soaked crystals were transferred into the mother liquor with additional 20% ethylene glycol and flash frozen using liquid nitrogen.

4.6. Data collection, structure determination, and refinement

The X-ray diffraction data sets were collected on a RU-H3RHB generator/Raxis-IV++ detector (Rigaku) to a resolution of 2.5 Å for compound **1** co-crystal, and on a synchrotron radiation beamline (5.0.2) at the Advanced Light Source (ALS) in Berkeley, California, to a resolution of 2.55 Å for compound **2** co-crystal. The data were integrated using MOSFLM[27] and scaled in CCP4.[28] The structures were solved by molecular replacement with MOLREP[29] using a monomer of the published 11β-HSD1 structure (PDB code: 1XU9) as a search model. Several rounds of model building were done using Quanta (Accelrys). The program REFMAC in CCP4 was used for structural refinement. The atomic coordinates and structure factors have been deposited in the RCSB Protein Data Bank under accession code 3D4N for compound **1** and 3D5Q for compound **2**.

Acknowledgments

We thank Donglin Guo for assistance in the construction and purification of recombinant human 11β-HSD1 from a baculovirus expression system. The Advanced Light Source (ALS) is supported by the Director, Office of Science, Office of Basic Sciences, Materials Sciences Division, of the U.S. Department of Energy under Contract No. DE-AC03-76SF00098 at the Lawrence Berkeley National Laboratory.

References and notes

1. Mariniello, B.; Ronconi, V.; Rilli, S.; Bernante, P.; Boscaro, M.; Mantero, F.; Giacchetti, G. *Eur. J. Endocrinol.* **2006**, *155*, 435–441.
2. Bujalska, I. J.; Kumar, S.; Stewart, P. M. *Lancet* **1997**, *349*, 1210–1213.
3. Seckl, J. R.; Walker, B. R. *Endocrinology* **2001**, *142*, 1371–1376.
4. Masuzaki, H.; Paterson, J.; Shinyama, H.; Morton, N. M.; Mullins, J. J.; Seckl, J. R.; Flier, J. S. *Science* **2001**, *294*, 2166–2170.
5. Andrews, R. C.; Rooyackers, O.; Walker, B. R. *J. Clin. Endocrinol. Metab.* **2003**, *88*, 285–291.
6. Alberts, P.; Nilsson, C.; Selen, G.; Engblom, L. O.; Edling, N. H.; Norling, S.; Klingstrom, G.; Larsson, C.; Forsgren, M.; Ashkzari, M.; Nilsson, C. E.; Fiedler, M.; Bergqvist, E.; Ohman, B.; Bjorkstrand, E.; Abrahmsen, L. B. *Endocrinology* **2003**, *144*, 4755–4762.
7. Hermanowski-Vosatka, A.; Balkovec, J. M.; Cheng, K.; Chen, H. Y.; Hernandez, M.; Koo, G. C.; Le Grand, C. B.; Li, Z.; Metzger, J. M.; Mundt, S. S.; Noonan, H.; Nunes, C. N.; Olson, S. H.; Pikounis, B.; Ren, N.; Robertson, N.; Schaeffer, J. M.; Shah, K.; Springer, M. S.; Strack, A. M.; Strowski, M.; Wu, K.; Wu, T.; Xiao, J.; Zhang, B. B.; Wright, S. D.; Thieringer, R. *J. Exp. Med.* **2005**, *202*, 517–527.
8. Tomlinson, J. W. *Minerva Endocrinol.* **2005**, *30*, 37–46.
9. Stulnig, T. M.; Waldhausl, W. *Diabetologia* **2004**, *47*, 1–11.
10. Walker, B. R.; Seckl, J. R. *Expert Opin. Therap. Targets* **2003**, *7*, 771–783.
11. Oppermann, U. *Endocr. Metab. Immune Disord. Drug Targets* **2006**, *6*, 259–269.
12. Olson, S.; Aster, S. D.; Brown, K.; Carbin, L.; Graham, D. W.; Hermanowski-Vosatka, A.; LeGrand, C. B.; Mundt, S. S.; Robbins, M. A.; Schaeffer, J. M.; Slossberg, L. H.; Szymonifka, M. J.; Thieringer, R.; Wright, S. D.; Balkovec, J. M. *Bioorg. Med. Chem. Lett.* **2005**, *15*, 4359–4362.
13. Richards, S.; Sorensen, B.; Jae, H.-s. J.; Winn, M.; Chen, Y.; Wang, J.; Fung, S.; Monzon, K.; Frevert, E. U.; Jacobson, P.; Sham, H.; Link, J. T. *Bioorg. Med. Chem. Lett.* **2006**, *16*, 6241–6245.
14. Gu, X.; Dragovic, J.; Koo, G. C.; Koprak, S. L.; LeGrand, C.; Mundt, S. S.; Shah, K.; Springer, M. S.; Tan, E. Y.; Thieringer, R.; Hermanowski-Vosatka, A.; Zokian, H. J.; Balkovec, J. M.; Waddell, S. T. *Bioorg. Med. Chem. Lett.* **2005**, *15*, 5266–5269.
15. Rohde, J.; Pliushchev, M.; Sorensen, B.; Wodka, D.; Shuai, Q.; Wang, J.; Fung, S.; Monzon, K.; Chiou, W.; Pan, L.; Deng, X.; Chovan, L.; Ramaiya, A.; Mullally, M.; Henry, R.; Stolarik, D.; Imade, H.; Marsh, K.; Beno, D.; Fey, T.; Droz, B.; Brune, M.; Camp, H.; Sham, H.; Frevert, E.; Jacobson, P.; Link, J. *J. Med. Chem.* **2007**, *50*, 149–164.
16. St. Jean, D. J., Jr.; Yuan, C.; Bercot, E. A.; Cupples, R.; Chen, M.; Fretland, J.; Hale, C.; Hungate, R. W.; Komorowski, R.; Veniant, M.; Wang, M.; Zhang, X.; Fotsch, C. *J. Med. Chem.* **2007**, *50*, 429–432.
17. Sun, D.; DeGraffenreid, M.; He, X.; Jaen, J. C.; Powers, J. P.; Yan, X.; Di, Y.; Tu, H.; Ursu, S.; Ma, J.; Miao, S.; Tang, L.; Ye, Q.; Sudom, A.; Wang, Z. Discovery and optimization of arylsulfonamides as a novel class of 11b-HSD1 inhibitors; 234th ACS National Meeting, 2007, Boston, MA, United States.
18. Julian, J. D.; Bostick, T.; Caille, S.; Chan, H.; Degraffenreid, M.; He, X.; Hungate, R. W.; Jaen, J. C.; Jiang, B.; Kaizerman, J.; Liu, J.; McMinn, D.; Powers, J. P.; Rew, Y.; Sudom, A.; Sun, D.; Tu, H.; Ursu, S.; Wang, Z.; Yan, X.; Ye, Q. Discovery and biological evaluation of novel benzamide derivatives as potent 11b-HSD1 inhibitors for the treatment of type II diabetes; 234th ACS National Meeting, 2007, Boston, MA, USA.
19. Cardozo, M. G.; Powers, J. P.; Goto, H.; Harada, K.; Imamura, K.; Kakutani, M.; Matsuda, I.; Ohe, Y.; Yata, S. *PCT Int. Appl.* **2005**. pp. WO-05044192.
20. Hosfield, D. J.; Wu, Y.; Skene, R. J.; Hilgers, M.; Jennings, A.; Snell, G. P.; Aertgeerts, K. *J. Biol. Chem.* **2005**, *280*, 4639–4648.
21. Ghosh, D.; Pletnev, V. Z.; Zhu, D. W.; Wawrzak, Z.; Duax, W. L.; Pangborn, W.; Labrie, F.; Lin, S. X. *Structure* **1995**, *3*, 503–513.
22. Nahoum, V.; Gangloff, A.; Legrand, P.; Zhu, D. W.; Cantin, L.; Zhorov, B. S.; Luu-The, V.; Labrie, F.; Breton, R.; Lin, S. X. *J. Biol. Chem.* **2001**, *276*, 42091–42098.
23. Sawicki, M. W.; Erman, M.; Puranen, T.; Vihko, P.; Ghosh, D. *Proc. Natl. Acad. Sci. U.S.A.* **1999**, *96*, 840–845.
24. Ogg, D.; Elleby, B.; Norstrom, C.; Stefansson, K.; Abrahmsen, L.; Oppermann, U.; Svensson, S. *J. Biol. Chem.* **2005**, *280*, 3789–3794.
25. Zhang, J.; Osslund, T. D.; Plant, M. H.; Clogston, C. L.; Nybo, R. E.; Xiong, F.; Delaney, J. M.; Jordan, S. R. *Biochemistry* **2005**, *44*, 6948–6957.
26. Draper, N.; Walker, E. A.; Bujalska, I. J.; Tomlinson, J. W.; Chalder, S. M.; Arlt, W.; Lavery, G. G.; Bedendo, O.; Ray, D. W.; Laing, I.; Malunowicz, E.; White, P. C.; Hewison, M.; Mason, P. J.; Connell, J. M.; Shackleton, C. H.; Stewart, P. M. *Nat. Genet.* **2003**, *34*, 434–439.
27. Leslie, A. G. W. Recent changes to the MOSFLM package for processing film and image plate data; Joint CCP4 + ESF-EAMCB Newsletter on Protein Crystallography, 1992.
28. Collaborative Computational Project, No 4. Acta Crystallogr. 1994, D50, 760–763.
29. Vagin, A.; Teplyakov, A. *J. Appl. Crystallogr.* **1997**, *30*, 1022–1025.